

# Low Temperature Growth of Boron Nitride Nanotubes on Substrates

Jiesheng Wang,<sup>†</sup> Vijaya K. Kayastha,<sup>†</sup> Yoke Khin Yap,<sup>\*,†</sup> Zhiyong Fan,<sup>‡</sup> Jia G. Lu,<sup>‡</sup> Zhengwei Pan,<sup>§</sup> Iliia N. Ivanov,<sup>§</sup> Alex A. Puretzky,<sup>§</sup> and David B. Geohegan<sup>§</sup>

*Department of Physics, Michigan Technological University, 1400 Townsend Drive, Houghton, Michigan 49931, Department of Chemical Engineering and Materials Science & Department of Electrical Engineering and Computer Science, University of California—Irvine, Irvine, California 92679, and Condensed Matter Sciences Division, Oak Ridge National Laboratory, Oak Ridge, Tennessee 37831*

Received September 16, 2005; Revised Manuscript Received October 27, 2005

## ABSTRACT

High growth temperatures (>1100 °C), low production yield, and impurities have prevented research progress and applications of boron nitride nanotubes (BNNTs) in the past 10 years. Here, we show that BNNTs can be grown on substrates at 600 °C. These BNNTs are constructed of high-order tubular structures and can be used without purification. Tunneling spectroscopy indicates that their band gap ranges from 4.4 to 4.9 eV.

Boron nitride nanotubes (BNNTs) were first predicted in 1994<sup>1,2</sup> and experimentally realized in the following year.<sup>3</sup> They are structurally similar to carbon nanotubes (CNTs) and exhibit extraordinary mechanical properties.<sup>4–6</sup> Despite these similarities, BNNTs are different from CNTs in other aspects. They possess uniform electronic properties that are insensitive to their diameters and chiralities.<sup>1,2</sup> Theoretically, their band gaps (~5 eV) are tunable and can even be eliminated by transverse electric fields through the giant dc Stark effect.<sup>7–9</sup> In addition, BNNTs demonstrate high oxidation resistance up to 800 °C,<sup>10</sup> excellent piezoelectricity,<sup>11,12</sup> and present potential material for room-temperature hydrogen storage.<sup>13</sup> Superlattices or isolated CNTs/BNNTs junctions<sup>14</sup> are predicted to produce itinerant ferromagnetism and spin polarization.<sup>15</sup> These properties make BNNTs very attractive for innovative applications in various branches of science.

Growing BNNTs is challenging. In the last 10 years, BNNTs were grown by arc discharge,<sup>3,16,17</sup> laser ablation,<sup>18,19</sup> substitution reactions from carbon nanotubes,<sup>20</sup> ball-milling,<sup>21</sup> and chemical vapor deposition (CVD),<sup>22</sup> at temperatures from 1100 to 3000 °C. These BNNTs were dominated by impurities including amorphous boron nitride (a-BN) powders and other solid-state byproducts. It is impossible to use these techniques to directly grow BNNTs on substrates for

device fabrication. High growth temperatures, low production yield, and contamination prevent large-scale synthesis and applications of BNNTs.

We grow BNNTs directly on substrates at 600 °C by a plasma-enhanced pulsed-laser deposition (PE-PLD) technique (see Supporting Information and Figure 1S). A negative substrate bias voltage induced by a nitrogen rf-plasma<sup>23,24</sup> generates the reactive condition for growing BNNTs. This substrate bias accelerates the positive ions in the rf plasma and the BN vapor to bombard on the substrate surface. When the kinetic energies of these ions are sufficient, the deposition rate of boron nitride (BN) films is balanced by the rate of resputtering and result in total resputtering. The growth of BNNTs is highly reproducible under this condition, which happened in our experiments when the substrate bias is between -360 and -450 V.

Scanning electron microscopy (SEM) indicates that multiple BNNTs grown from adjacent Fe catalyst particles tend to form vertical bundles. BNNTs grown at -380 V appear in conical features as shown in Figure 1A. For samples grown at higher substrate bias (-450 V), individual BNNTs inside the bundles can clearly be resolved (Figure 1B). This is because of the increase of the diameters (~20 nm) of individual BNNTs as grown from larger Fe nanoparticles that formed by the enhanced plasma heating. The charging effect in SEM prevents the resolution of individual BNNTs with smaller diameters due to the insulating nature of the BNNTs. The bundling configurations of BNNTs with small and big diameters are schematically drawn in Figure 1C (left

\* Corresponding author. E-mail: ykyap@mtu.edu.

<sup>†</sup> Department of Physics, Michigan Technological University.

<sup>‡</sup> Department of Chemical Engineering and Materials Science & Department of Electrical Engineering and Computer Science, University of California—Irvine.

<sup>§</sup> Condensed Matter Sciences Division, Oak Ridge National Laboratory.

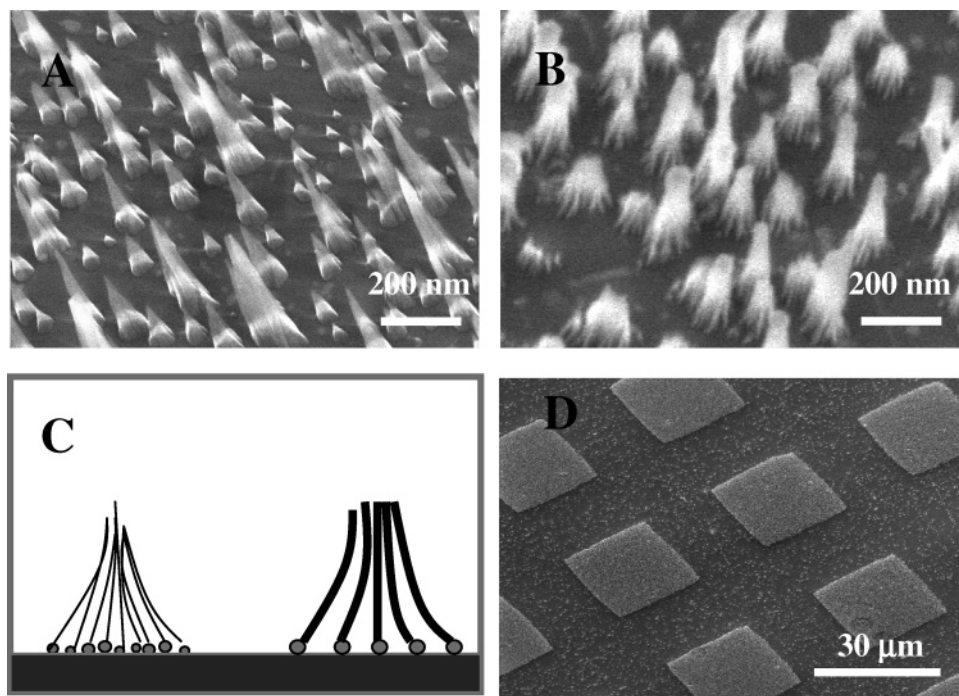


**Figure 1.** SEM images of BNNT bundles grown at a substrate bias of (A)  $-380$  V and (B)  $-450$  V and (C) their corresponding bundling configurations (left and right, respectively). (D) Patterned growth of BNNTs.

and right, respectively). These BNNT bundles can be grown into arrays of regular patterns (Figure 1D) with a patterned Fe film created by a shadow mask. These results indicate that the growth location of BNNTs is controllable by the patterns of the Fe nanoparticles, like the catalytic growth of CNTs by CVD techniques.

Transmission electron microscopy (TEM) was used to examine the structure of the BNNTs. Long and straight tubular structures were detected (Figure 2A). The tips of these BNNTs were fully capped with no evidence of catalyst particles. This observation indicates that base-growth mechanism is responsible for the growth of the BNNT bundles. A magnified image (Figure 2B) indicates that these BNNTs are made of high-order hexagonal phase BN (h-BN) shells with intershell spacing of  $0.333$  nm. The internal tubular channel of these BNNTs can be as small as  $\sim 1$  nm. Another intrinsic structure of BNNTs is identified from this image, i.e., some BNNTs are found to have squarelike cross-section caps, which are typical for high-quality BNNTs.<sup>17,25</sup> The h-BN shells of BNNTs can form squarelike caps as a result of the stable  $B_2N_2$  rings. The occurrence of a single four-member ring tends to lead to closure by a sharp and relatively square cross-section cap. Selective area diffraction was performed on three adjacent BNNTs (Figure 2C). Three pairs of bright spots (Figure 2D) from (002) and (004) planes of the three BNNTs are clearly observed and indicate the high structural order of these BNNTs.

The growth of these BNNTs is obtained through an optimum combination of the Fe film thickness, the laser energy density (deposition rate), and the substrate bias. For example, for substrate with  $12.5$  nm thick Fe film at a substrate bias of  $-300$  V, excessive deposition rate results in the coating of BN films on the Fe nanoparticles (Figure

3A and Figure 4A). The insulating BN coatings can be recognized by the charging effect during the SEM measurement. The growth of BNNTs is difficult to identify in these cases. At this condition, the deposition rate of BN films is faster than the diffusion rate of the BN growth species into the Fe catalyst particles. Thus BN films coated on the catalyst terminate the contact between Fe and the reactive growth species (Figure 3A). This phenomenon is referred to as the poisoning effect in the growth of CNTs.<sup>26</sup> The thickness of BN films gradually reduces with an increase in the substrate bias (Figure 3B). BNNTs start to grow as a balance of film deposition rate and resputtering rate occurs at higher substrate bias (Figure 3C). At this total resputtering region, the deposition of BN thin films is suppressed. BNNTs are grown on the Fe nanoparticles according to the vapor–liquid–solid mechanism.<sup>27</sup> The rf plasma creates a directional flux of the BN growth species with sufficient kinetic energies to diffuse into the Fe nanoparticles. Thus, Fe serves to capture the energetic BN growth species and confine them in a nanoscopic space. Otherwise, these species are resputtered off. When the Fe nanoparticles become supersaturated with BN vapor, the BN species condense into the ordered nanotubular structures.

In contrast, when no laser ablation was applied, simply by blocking the laser pulses from ablating the BN target, no BNNTs and BN films were deposited (Figure 4B). Most Fe particles are sputtered away since there was no BN species deposited to compensate the sputtering process. In addition, we found that BNNTs are not grown when Si substrates were used. We believe that iron silicides could have formed due to the absence of the oxide diffusion barrier that maintains the integrity of the Fe nanoparticles at the nucleation stage of BNNTs.

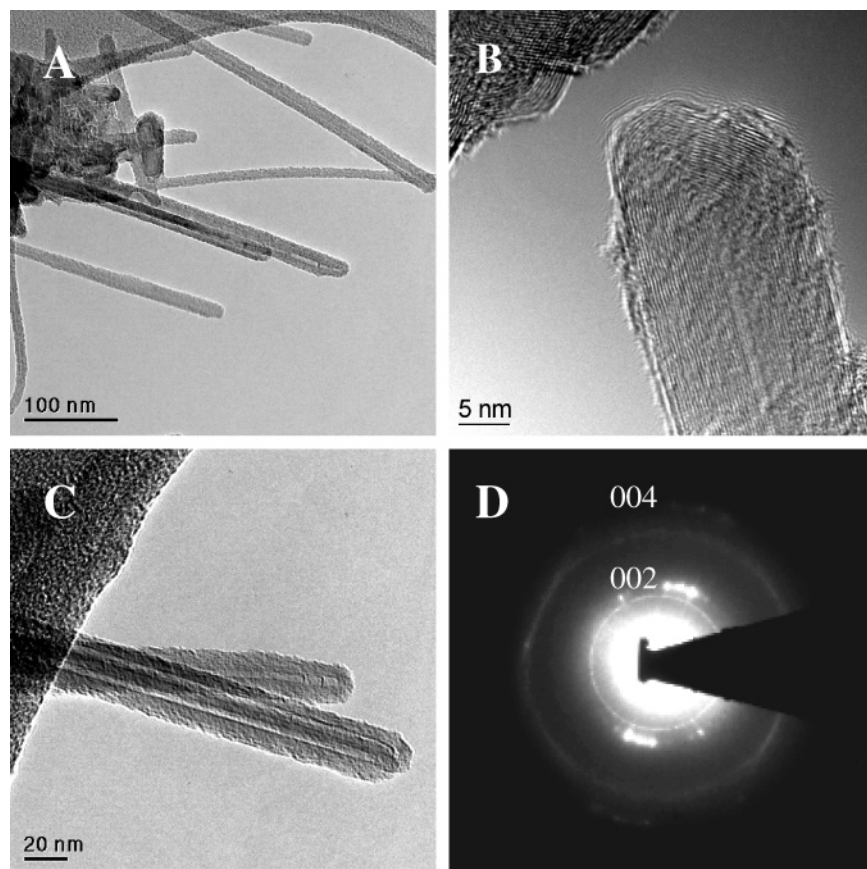


**Figure 2.** TEM images of BNNTs at (A) low and (B) high magnifications. (C) Images of three adjacent BNNTs and their (D) corresponding diffraction patterns.

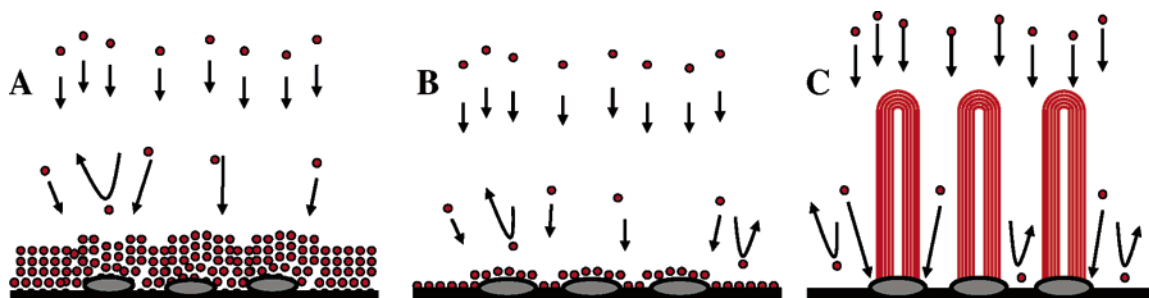


**Figure 3.** Schematic drawing representing the growth region of BNNTs. (A) Deposition of BN films on Fe nanoparticles due to low resputtering rate of the growth species. (B) Reduced growth rate of BN films from energetic growth species. (C) Total resputtering region where BNNTs are grown and BN films are suppressed.

We then examined the local density of electronic states (LDOS) of the BNNTs. Tunneling spectroscopy by scanning probe microscopy is frequently used to understand the surface electronic states of various semiconductors including BNNTs.<sup>28,29</sup> The bulk band gap is revealed from these LDOS spectra since dangling bond states on the surface do not appear in the gap. We measured the LDOS spectra of BNNTs at room temperature with an atomic force microscope (AFM) with Ti–Pt coated conductive probes in conjunction with an external data acquisition system.

Figure 5A shows a contact mode AFM image ( $5 \times 5 \mu\text{m}^2$ ) with bright grains representing the BNNT bundles. The electrical measurement was conducted by placing the AFM probe on the tips of these BNNTs (inset of Figure 5B). Current–voltage ( $I$ – $V$ ) curves (Figure 5B) were obtained

on the BNNTs (T in Figure 5A) and the substrate surface (S in Figure 5A) by applying bias voltages on the AFM probe. These curves show a larger conductance of the substrate, which indicates that most of the oxide layers were etched away during the growing process. It also proves that no significant BN films were deposited on the substrates, consistent with the earlier discussion that BNNTs are grown in the total resputtering region.

Differential conductance measurements ( $dI/dV$ ) of BNNTs were acquired concurrently with the measurement of the  $I$ – $V$  curves using the lock-in amplifier in the measurement setup. The  $dI/dV$  data from BNNT and substrate (Figure 5C) were first obtained and then subtracted to yield the net data for BNNTs by considering the resistances of BNNT and

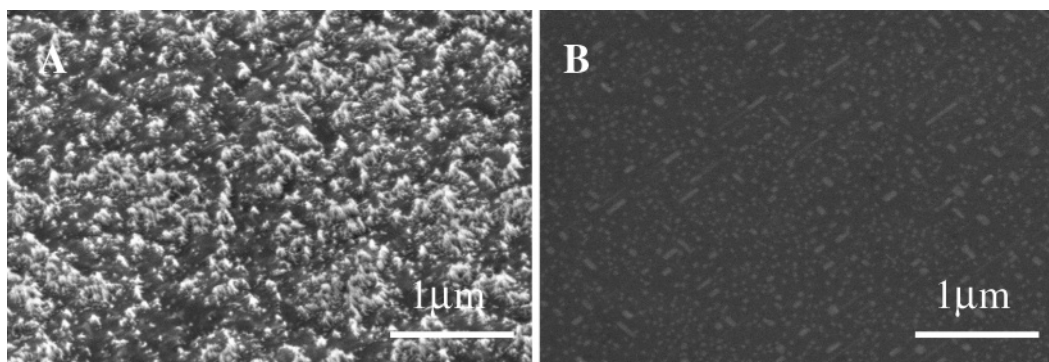


**Figure 4.** (A) SEM image of a sample deposited at low substrate bias ( $-300$  V). Iron particles coated with BN films are detected. (B) SEM image of sample prepared without the deposition of boron nitride plume (simply plasma treatment at substrate bias of  $-400$  V). Most Fe particles are sputtered away.

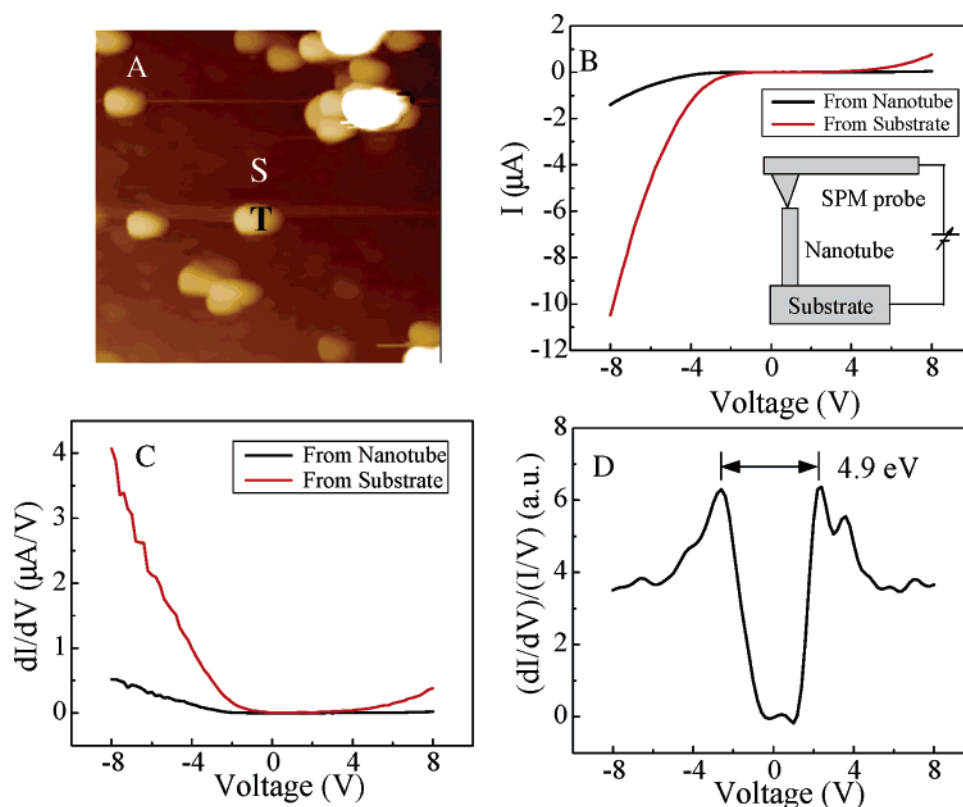


**Figure 5.** (A) AFM images of the vertically aligned BNNT bundles. T and S representing BNNTs and substrate surface, respectively. (B)  $I/V$  curve obtained from point T (black curve) and S (red curve). Inset shows the related measurement setup. (C)  $dI/dV$  curves obtained from the point T (black curve) and S (red curve). (D) Normalized differential conductance for BNNTs representing their LDOS and a band gap of  $\sim 4.9$  eV.

substrate are in series. The subtracted  $dI/dV$  and  $I/V$  data are then used to obtain the normalized differential conductance (Figure 5D). The normalized differential conductance for our BNNTs indicates two major peaks at positive and negative bias voltages, corresponding to the edges of the valence band and conduction band, respectively. The separation of these peaks gives an estimation of the energy band gap of  $\sim 4.9$  eV, which is similar to the reported experimental data for BNNTs.<sup>29</sup> The detected band gaps from our measured spectra varied from 4.4 to 4.9 eV. LDOS spectra obtained here are the first successful case conducted by flowing current along the axes of the vertically aligned BNNTs.

In summary, results shown here will form the basis for future investigation of BNNTs including large-scale synthesis, doping, and the growth of BN/carbon nanotubular junctions.

**Acknowledgment.** Y.K.Y. thanks support from Michigan Tech Research Excellence Fund, the U.S. Department of Army (Grant No. W911NF-04-1-0029, through the City College of New York), the National Science Foundation CAREER award (Award No. 0447555, Division of Materials Research), and the Center for Nanophase Materials Sciences sponsored by the Division of Materials Sciences and

Engineering, U.S. Department of Energy, under Contract No. DE-AC05-00OR22725 with UT-Battelle, LLC. J.G.L. thanks support from the National Science Foundation CAREER award (Award No. ECS 0306735) and NIRT Grant No. 78608.

**Supporting Information Available:** A description of the experimental procedures and a schematic of the PE-PLD system. This material is available free of charge via the Internet at <http://pubs.acs.org>.

## References

- (1) Rubio, A.; Corkill, J. L.; Cohen, M. L. *Phys. Rev. B* **1994**, *49*, 5081.
- (2) Blase, X.; Rubio, A.; Louie, S. G.; Cohen, M. L. *Europhys. Lett.* **1994**, *28*, 335.
- (3) Chopra, N. G.; et al. *Science* **1995**, *269*, 966.
- (4) Hernández, E.; Goze, C.; Bernier, P.; Rubio, A. *Phys. Rev. Lett.* **1998**, *80*, 4502.
- (5) Kudin, K. N.; Scuseria, G. E.; Yakobson, B. I.; *Phys. Rev. B* **2001**, *64*, 235406.
- (6) Suryavanshi, A. P.; et al. *Appl. Phys. Lett.* **2004**, *84*, 2527.
- (7) Khoo, K. H.; Mazzoni, M. S. C.; Louie, S. G. *Phys. Rev. B* **2004**, *69*, 201401(R).
- (8) Chen, C.-W.; Lee, M.-H.; Clark, S. J. *Nanotechnology* **2004**, *15*, 1837.
- (9) Ishigami, M.; Sau, J. D.; Aloni, S.; Cohen, M. L.; Zettl, A. *Phys. Rev. Lett.* **2005**, *94*, 56804.
- (10) Chen, Y.; Zou, J.; Campbell, S. J.; Caer, G. L. *Appl. Phys. Lett.* **2004**, *84*, 2430.
- (11) Mele, E. J.; Král, P. *Phys. Rev. Lett.* **2002**, *88*, 56803.
- (12) Nakhmanson, S. M.; Calzolari, A.; Meunier, V.; Bernholc, J.; Nardelli, M. B. *Phys. Rev. B* **2003**, *67*, 235406.
- (13) Jhi, S. H.; Kwon, Y. K. *Phys. Rev. B* **2004**, *69*, 245407.
- (14) Blase, X.; Charlier, J.-C.; De Vita, A.; Car, R. *Appl. Phys. Lett.* **1997**, *70*, 197.
- (15) Choi, J.; Kim, Y.-H.; Chang, K. J.; Tománek, D. *Phys. Rev. B* **2003**, *67*, 125421.
- (16) Terrones, M.; et al. *Chem. Phys. Lett.* **1996**, *259*, 568.
- (17) Loiseau, A.; Willaime, F.; Demoncy, N.; Hug, G.; Pascard, H. *Phys. Rev. Lett.* **1996**, *76*, 4737.
- (18) Yu, D. P. et al. *Appl. Phys. Lett.* **1998**, *72*, 1966.
- (19) Lee, R. S.; et al. *Phys. Rev. B* **2001**, *64*, 121405 (R).
- (20) Han, W.; Bando, Y.; Kurashima, K.; Sato, T. *Appl. Phys. Lett.* **1998**, *73*, 3085.
- (21) Chen, Y.; Chadderton, L. T.; Gerald, J. F.; Williams, J. S. *Appl. Phys. Lett.* **1999**, *74*, 2960.
- (22) Lourie, O. R.; et al. *Chem. Mater.* **2000**, *12*, 1808.
- (23) Yap, Y. K.; Yoshimura, M.; Mori, Y.; Sasaki, T. *Appl. Phys. Lett.* **2002**, *80*, 2559.
- (24) Yap, Y. K.; Kida, S.; Aoyama, T.; Mori, Y.; Sasaki, T. *Appl. Phys. Lett.* **1998**, *73*, 915.
- (25) Golberg, D.; et al. *J. Appl. Phys.* **1999**, *86*, 2364.
- (26) Kayastha, V.; Yap, Y. K.; Dimovski, S.; Gogotsi, Y. *Appl. Phys. Lett.* **2004**, *85*, 3265.
- (27) Wagner, G. W.; Ellis, W. C. *Appl. Phys. Lett.* **1964**, *4*, 89.
- (28) Feenstra, R. M. *Phys. Rev. B* **1994**, *50*, 4561.
- (29) Czerw, R.; et al. *Appl. Phys. Lett.* **2003**, *83*, 1617.

NL051859N